ISSN 0001-4338, Izvestiya, Atmospheric and Oceanic Physics, 2015, Vol. 51, No. 4, pp. 362–380. © Pleiades Publishing, Ltd., 2015.
Original Russian Text © K.V. Ushakov, R.A. Ibrayev, V.V. Kalmykov, 2015, published in Izvestiya AN. Fizika Atmosfery i Okeana, 2015, Vol. 51, No. 4, pp. 416–436.

Simulation of the World Ocean Climate with a Massively Parallel Numerical Model[1]

K. V. Ushakov[a, b, c, d], R. A. Ibrayev[a, b, c, d], and V. V. Kalmykov[a, b, c, e]

[a] *Shirshov Institute of Oceanology, Russian Academy of Sciences, Nakhimovskii pr. 36, Moscow, 117987 Russia*
e-mail: ushakovkv@mail.ru

[b] *Institute of Numerical Mathematics, Russian Academy of Sciences, ul. Gubkina 8, 119333 Russia*

[c] *Hydrometeorological Research Center of the Russian Federation, Bol'shoi Predtechensky per. 11-13, Moscow, 123242 Russia*

[d] *Moscow Institute of Physics and Technology, Instituskii per. 9, Dolgoprudnyi, Moscow Oblast', 141700 Russia*

[e] *Moscow State University, Moscow, 119991 Russia*

Received October 30, 2014; in final form, November 11, 2014

Abstract—The INM-IO numerical World Ocean model is verified through the calculation of the model ocean climate. The numerical experiment was conducted for a period of 500 years following the CORE-I protocol. We analyze some basic elements of the large-scale ocean circulation and local and integral characteristics of the model solution. The model limitations and ways they are overcome are described. The results generally fit the level of leading models. This experiment is a necessary step preceding the transition to high-resolution diagnostic and prognostic calculations of the state of the World Ocean and its individual basins.

Keywords: World Ocean, climate, global circulation, numerical models, CORE-I experiment
DOI: 10.1134/S0001433815040131

1. INTRODUCTION

Numerical models of the ocean general circulation have been used for more than fifty years to study the ocean dynamics, the Earth's climate as a whole, and their variability on different spatial and temporal scales [1–3]. Over this time period, the resolution of models has increased two orders of magnitude (from several degrees to hundredths of a degree) and the parameterization of physical processes has been significantly improved. Here, each stage of the progress posed a problem of the verification and calibration of models by comparing with observation data on appropriate spatial and temporal scales (from global climatic characteristics of the ocean to the synoptic variability of mesoscale eddies and jet currents).

The program code of a model suitable for both climate studies and weather forecasts should provide operation in a wide range of spatial scales. For example, a recent IPCC report [4] suggests a horizontal resolution of ocean models of 1°–0.5°. At the same time, a number of studies showed that, to describe mesoscale eddies and dynamic structures of the ocean (such as the Gulf Stream [5, 6] and the currents in the straits between Europe and Greenland [7]), the horizontal resolution must be no less than (1/10)°. The calculations of the entire World Ocean with this high resolution require efficiently scalable numerical algorithms and powerful supercomputers. At present, activities of this kind are conducted by three research groups: Los Alamos National Laboratory, Naval Postgraduate School, United States (POP model [8]); Earth Simulator Center, Japan (OFES model based on MOM [9]); and the European Community DRAKKAR program (NEMO model [10]). The Russian INMOM ocean model [11] contributing to the report [4] currently has a number of specific structural features that do not allow the model to be run on the massively parallel computing systems.

In view of this, the Institute of Numerical Mathematics of the Russian Academy of Sciences and the Shirshov Institute of Oceanology of the Russian Academy of Sciences initiated research on creating a high-resolution model of the global ocean. This model was based on the model of enclosed sea hydrodynamics [12]. The new model involved significant modifications. First, the shallow water equations are solved using an explicit scheme [13] to find the barotropic components of currents. A unique fast algorithm was proposed for solving shallow-water equations on par-

[1] The paper is dedicated to the memory of Academician G.I. Marchuk.

allel computers with distributed memory [14]. In addition, new technologies were developed for parallel exchanges, multilevel data interpolation, and asynchronous treatment of the file system, which outperformed their foreign counterparts (CESM cpl7, MCT, OASIS) in terms of the efficient use of supercomputing resources [15–18]. The first results of the run of the new model of the World Ocean dynamics on grids with a horizontal resolution of ((1/10)°) and 49 vertical levels (INM–IO model $1/10 \times 1/10 \times 49$ [19, 20]) show that the computing technologies developed are correct and efficient and can be used for the explicit simulation of a wide range of physical processes in the ocean. At the same time, it should be recognized that the detailed testing of high-resolution global ocean models requires very large computing resources. Therefore, it is still desirable to test the numerical schemes on models of a low (around 1°) horizontal resolution.

This paper presents the results of the first stage of the verification of the INM–IO World Ocean model with a resolution of 0.5°. The verification was conducted through a numerical experiment for a simulation period of 500 years; the initial state was represented by the climatological distribution of temperature and salinity and the temporal dynamics of external forcing was specified by a cyclic repetition of the CORE-I "normal" year [21]. In Russia, a similar experiment with interannual variability of the forcing was conducted by the authors of [11].

Section 2 presents the main features of the INM–IO model. Section 3 describes the setup of the numerical experiment and the values of model parameters used. Section 4 demonstrates the results of the experiment and a number of spatial and integral characteristics of the solution, providing a comparison between observed data and the results of models involved officially in the CORE-I experiment. Section 5 presents the conclusions drawn from this study and projects further lines of model improvement.

2. THE INM–IO OCEAN MODEL

The INM–IO World Ocean model is a software package designed for analyzing the seawater circulation in a wide range of spatial and temporal scales. The complete system of equations of three-dimensional ocean dynamics in the Boussinesq and hydrostatic approximations is solved by a finite volume method on type B grid. Since this type of grid is characterized by a number of drawbacks (for example, a two-step noise in the ocean surface field), we plan to use a type C grid in the future. The vertical axis uses z coordinates. The barotropic dynamics is described with the help of a two-dimensional system of shallow-water equations by the scheme [13]. The state of sea ice is described by the thermodynamic model [22], and the heat, salt, momentum, and water flows on the atmospheric boundary are calculated by the boundary layer model [23]. Horizontal turbulent mixing is described using the hypothesis that the turbulence flows are proportional to the gradients of transferred substances (temperature, salinity, and momentum). Additionally, these fields are smoothed by a biharmonic filter. The corresponding coefficients of diffusion and viscosity are constant. Vertical mixing is parameterized by the Munk–Anderson scheme [24]. These simple parameterizations were used as the first step of model development and in the future will be replaced by more advanced schemes or rejected as useless when an increased resolution is used. The surface of the air–water interface is free, with an explicit description of water, heat, salt, and momentum flows.

Except for vertical turbulent mixing, all the processes were described using explicit numerical methods. This made it possible to perform a reasonable parallelization of the program code using the method of two-dimensional domain decomposition. Test calculations showed that the model is almost linearly scalable up to 32400 processor cores with a spatial resolution of (1/10)° and that the resolution can be increased up to (1/20)°. The data input–output was also fully parallelized using tools of the Framework for Coupled Modeling [15–17].

The numerical schemes of water volume transport and heat and salt transport/diffusion are fully consistent, which ensures (when the format of data storage is real(8)) that the mean level of the ocean is conserved in this numerical experiment with an accuracy of 10^{-11} m, the value of vertical velocity at the bottom is within 10^{-15} m/s, and the mean values of temperature and salinity (in the test calculation for one year with no external flows) are conserved with an accuracy of 10^{-5} °C and 10^{-5} psu, respectively. The momentum transport is calculated using a central difference scheme and the heat and salt transfer is calculated using a flux-corrected scheme [25]. A more detailed description of the model and the first results of eddy-resolving calculations of the ocean state can be found in [19, 20].

3. SETUP OF THE NUMERICAL EXPERIMENT

In this paper, we describe a numerical experiment for calculating the proper climate in the ocean model under the effect of cyclically recurring (over a period of 500 years) "normal" annual variation in atmospheric parameters and solar radiation determined from the CNYFv2 database of the CORE-I protocol [26]. The wind velocity, air temperature, and humidity at a height of 10 m are specified with a resolution of 6 h; the longwave and shortwave downward surface radiation are daily mean values and the precipitation and continental runoff are monthly mean values. Here, to avoid a model drift, the surface salinity is drawn (relaxed) to the monthly mean PHC2 climatology [27] using an artificial salt flux proportional to the salinity anomaly with a factor of 50 m/4 years (in terms of [21], this value of the coefficient corresponds to weak

relaxation). After this, the flows of moisture and artificial salt are normalized (the global mean value is subtracted) at each time step.

The initial fields of temperature and salinity are the annual mean fields taken from the WOA2009 database [28], the initial values of current velocities are zero, and the sea ice is disregarded at the start of the experiment.

The horizontal system of coordinates is three-polar [29]. The grid resolution in the spherical part (south of 60° N) is 0.5°. The grid cell dimensions vary from 56 × 56 km at the equator to 12 × 56 km on the Antarctic coast, 15 × 33 km at the North Pole, and 21 × 16 km along the coasts of Siberia and Canada. On the boundary of spherical and bipolar grids, the longitudinal resolution varies continuously, and the latitudinal step jump is less than 15% for most of the boundary. The depth of the computational domain is piecewise constant and lies in the range of 12 to 6125 m. The bottom topography was taken from the ETOPO5 database [30]. The inland water areas and the Black Sea are disregarded in the calculations. There are 49 vertical levels with a step of 6 m in the upper layer to 250 m in the lower layer. The time step is 12 min for three-dimensional baroclinic equations and 0.6 min for shallow water equations.

The coefficients of turbulent exchange (viscosity and diffusion) were chosen so as to ensure the stability of computations and retain the variability of ocean dynamics as much as possible for the given resolution and time step. The horizontal viscosity coefficients for shallow-water equations and baroclinic dynamics are 1000 and 2500 m^2/s, respectively. The coefficients of horizontal biharmonic viscosity and diffusion are used only for baroclinic equations and constitute -1.25×10^{12} m^4/s. The coefficient of horizontal diffusion for heat and salt is 1000 m^2/s. The background values of vertical viscosity and diffusion are 10^{-4} and 10^{-6} m^2/s, respectively; their maximum values in areas with a small Richardson number are 10^{-2} and 10^{-3} m^2/s, respectively. The test experiments indicated that the horizontal exchange coefficients for most of the World Ocean can be significantly reduced; however, in this paper, we limit ourselves to a calculation with spatially constant coefficients.

The calculations were performed on the MVS10P computer of the Joint Supercomputer Center of the Russian Academy of Sciences. The number of processor cores used was 1615; here, the calculation for one model year took around 10 min of real time.

4. NUMERICAL EXPERIMENT RESULTS

This section analyzes the model capability to simulate the main elements of the global ocean climate circulation. We consider a number of diagnostic characteristics of the model solution and compare them with the results of other models, as well as observational and reanalysis data.

4.1. Change in Average Temperature and Salinity

The numerical experiment for a period of 500 years revealed that the mean temperature of the World Ocean has increased by approximately 0.1°C and reached a quasi-equilibrium value (hereafter, by temperature, we mean potential temperature relative to the ocean surface). The increase in mean salinity was around 0.03 psu with a residual trend of 0.004 psu for 100 years caused, as is shown by additional sensitivity experiments, by the unbalanced response by the ice model. Despite salinity drift, these results (Fig. 1) are sufficiently realistic and lie in the range of data scatter by the most widely used models mentioned in the CORE-I experiment review [21].

A more detailed presentation of the model spinup can be obtained by constructing plots of water properties as a function of time and depth. Figure 2 shows the temporal dynamics of deviations in annual mean temperature and salinity from WOA2009 annual mean climatological data. It can be seen that the temperature of surface waters and the thermocline becomes almost stabilized during the first 50 years, while the remaining waters retain a weak positive drift at depths of 300 to 1000 m and a negative drift at a depth of around 250 m. A similar distribution of temperature trends is observed in the calculations conducted with the POP, ORCA, and MPI z-coordinate models [21], while the temperature plots in models with and isopycnic or hybrid coordinates (HIM, MICOM, and HYCOM) are qualitatively different. Specifically, the isopycnic models are characterized by cooling of the entire oceanic column except the upper layer up to 300 m. It should be noted that during the preparation of this experiment, the upwind scheme used earlier for scalar transport was found to be completely unsuitable for long-term calculations because it leads to the unrealistic overheating of deep oceanic layers.

The plot of salinity shows a noticeable freshening with expressed interannual variations in the upper 500-m layer and a salinization center at depths of around 1000 m. Like in the case of temperature, this pattern is similar to the results of calculations conducted with z-coordinate models, with the difference that no freshening of deep waters is observed in this experiment.

In all sections except for 4.4 and 4.7, we consider the numerical experiment results averaged over 491–500 years.

4.2. Surface Temperature and Salinity

Figure 3 shows the deviations in surface temperature and salinity from the WOA2009 annual mean values. Despite the fact that these fields are rather rigidly fixed to a given atmospheric forcing, the internal model dynamics gives rise to a number of specific features.

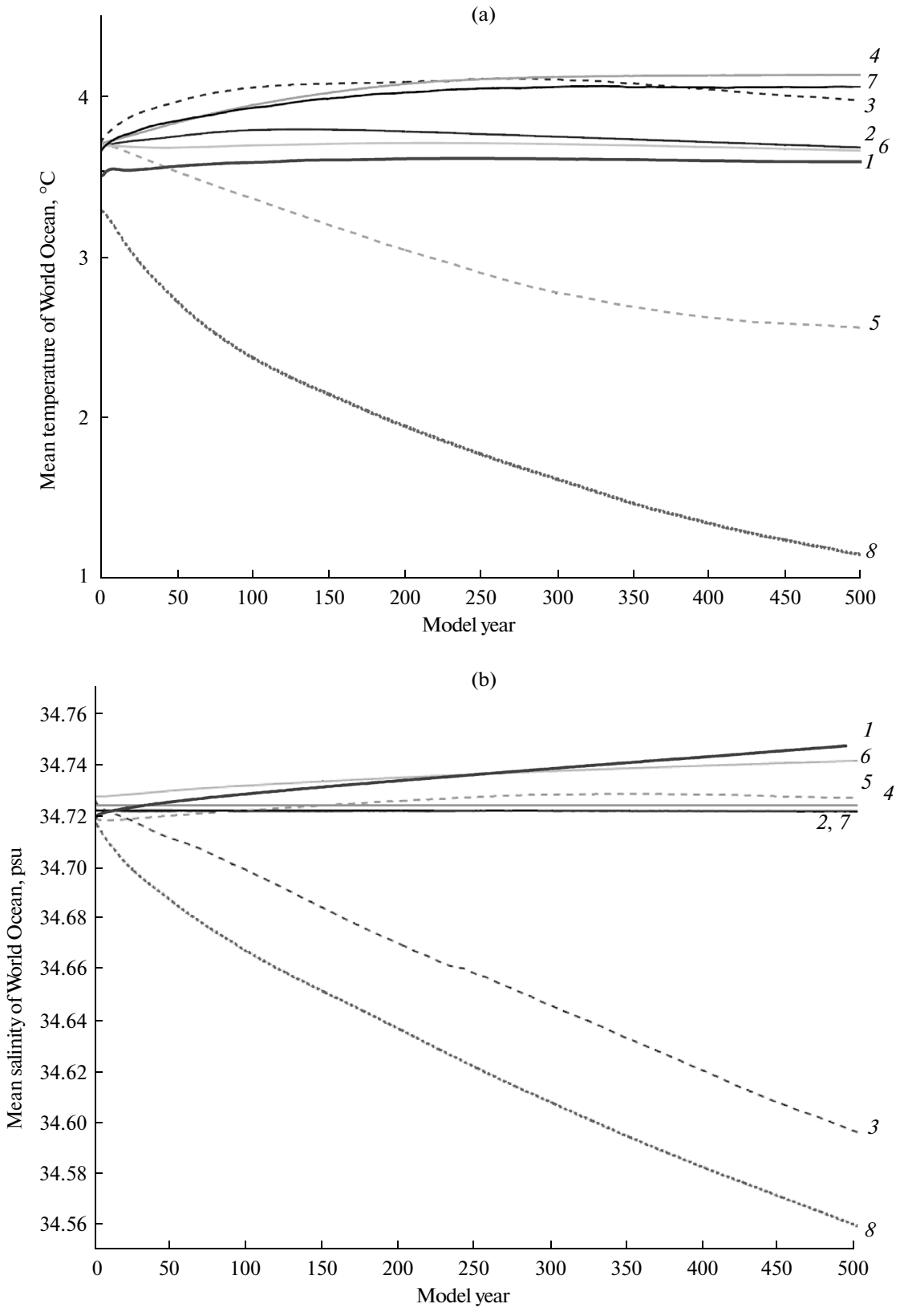

Fig. 1. Change in global annual average (a) temperature and (b) salinity during the numerical experiment in comparison with the results of the models of [21]. (*1*) INM–IO, (*2*) POP, (*3*) HYCOM, (*4*) MOM, (*5*) HIM, (*6*) ORCA, (*7*) MPI, and (*8*) MICOM.

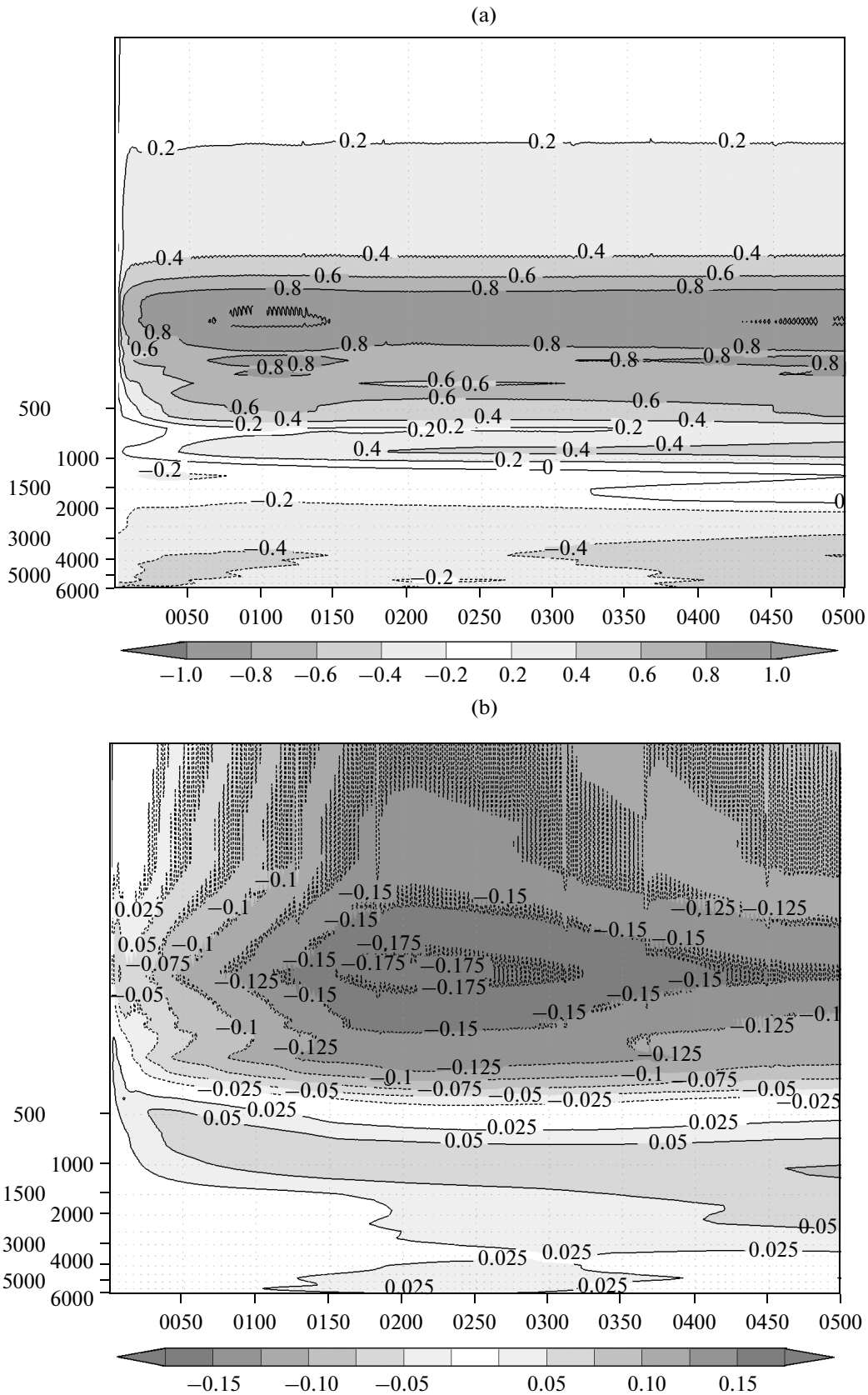

Fig. 2. Change in horizontally averaged (a) temperature (°C) and (b) salinity (psu) as a function of time (years) and depth (m) (deviation from the WOA2009 annual mean climatology). Hereafter, the dotted contours denote negative values.

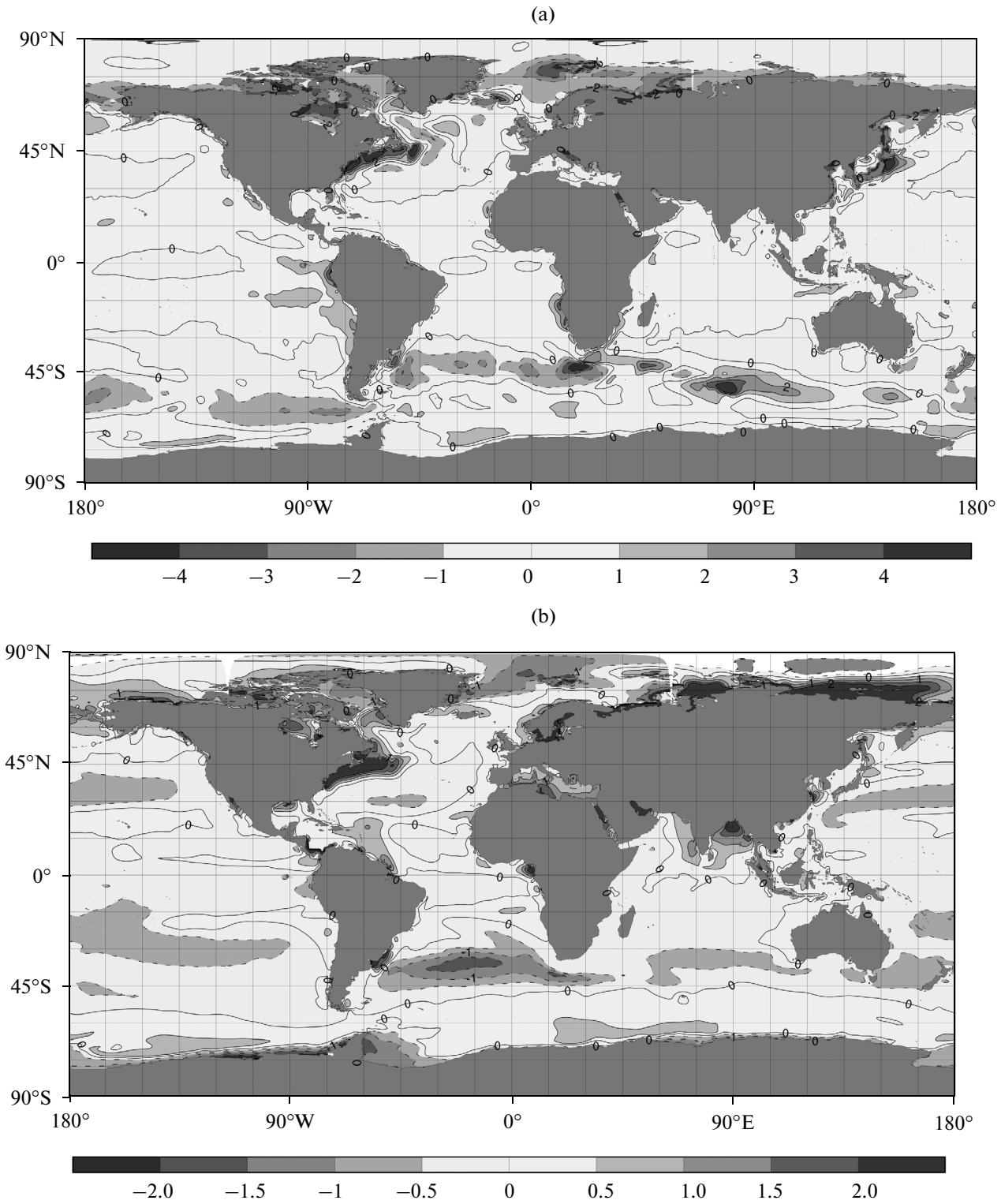

Fig. 3. Deviations of surface (a) temperature (°C) and (b) salinity (psu) from the WOA2009 annual average climatology.

Primarily, this refers to the expressed positive deviations north of frontal zones in the areas of western boundary currents (the Gulf Stream and Kuroshio). To simulate these currents, it is necessary to have a spatial resolution of no less than 0.1° (for example, see [5, 6, 9]); therefore, the resolution used by us (0.5°) inevitably leads to this kind of error. To one extent or another, these errors appear in all models covered by the review [21]. In [20], the quality of the simulation of the Gulf Stream current was demonstrated to

depend on the model resolution. Most likely, the lack of the resolution is responsible for the fact that the northward transport of freshened cold waters of the Falkland Current is blocked and the rate of rise of cold waters near the west coasts of Africa and South America is insufficient.

The model also fails to correctly simulate the location of the North Atlantic Current near the subpolar gyre, which manifests itself in the alternation of positive and negative temperature deviations and is probably the source of insufficient heat transfer into the Nordic Seas. The correction of these errors may require an adjusted parameterization of vertical mixing.

The extensive Arctic freshening points to the need for a more accurate model of sea ice, while the sharp positive deviations near the mouths of Siberian rivers may be indicative of errors in the specification of external atmospheric forcing or inconsistency between WOA2009 (the deviations are measured from these data) and PHC2 (used for calculating the relaxation salt flux) data.

The central regions of the Pacific, Indian, and Atlantic oceans are simulated with a sufficient adequacy. For example, the temperature deviations were comparable with the uncertainty of climatological data themselves (0.5–2°C in a number of areas [21]).

One of the most difficult regions for the model was the Southern Ocean. The model solution for this ocean is characterized by extended zonal deviations of temperature and salinity. These deviations can be explained in part by uncertainty in climatological data. Indeed, according to the remark in [21], the surface temperatures for the African and Atlantic sectors of the Southern Ocean in [31] turn out to exceed the values obtained in [32] by 0.5–1°C. However, some diagnostic characteristics considered below point to the need for adjusting the model solution namely in this region.

4.3. Zonal Mean Temperature and Salinity

The distribution of temperature and salinity by latitude and depth directly reflects the intensity of the circulation and ventilation of deep waters. This distribution makes it possible to study processes such as the meridional transport of mass, heat, and salt, convective mixing, and carbon exchange, which cannot be easily measured directly.

Figure 4 shows the global zonal mean fields of temperature and salinity as deviations from the WOA2009 annual average fields. Like in most models [21], one can see heat areas in the upper layer of the tropical ocean. These areas are probably caused by the insufficiency of the model resolution to simulate equatorial upwelling (see subsection 4.9). The clearly expressed deviations at 40°–80° N point to an overly strong vertical exchange in these areas and can explain the deficit of heat transfer into the Arctic.

Conversely, the resulting Antarctic bottom water is significantly colder than the measured values. The numerical experiment yields an ice deficit in this area (subsection 4.5), which apparently leads to a reduced near-surface salinity; an increased heat emission into the atmosphere; and, accordingly, an intensified downward motion of cold waters and their northward transport at deeper layers (subsection 4.9).

The strong freshening in the upper 250-m layer at 25°–45° S generally follows the surface deviation from climatology. Although the reason remains unknown, we can note that, according to the results of [21], this proves to be typical for models with a weak relaxation of surface salinity.

4.4. Interannual Dynamics of Heat Content in the Upper Oceanic Layer

To estimate the quality of the simulation of the annual cycle of near-surface thermal characteristics of the ocean, we compare (see Fig. 5) the monthly average values of surface temperature and heat content (integrated temperatures over the vertical) of the upper 250-m layer for a number of model years and for WOA2009 data at the point 35° N, 48° W. The plot points corresponding to the months of the year are arranged counterclockwise from January to December. Figure 5b shows similar plots for the 50th year of modeling with the INM–IO and three other models described in [21]; here, the authors of the MPI model conducted experiments with strong and weak relaxation of surface salinity (the relaxation rates were 50 m/300 days and 50 m/4 years, respectively).

All these models qualitatively simulate the phase of seasonal heat-content oscillations; during the processing of the results of our experiment, we revealed that the phase errors of the models have the same order of magnitude as the differences between different climatological data (for example, between PHC3.0 and WOA2001 with a resolution of 0.25°). However, the average value and amplitude of heat content proved to be significantly underestimated in comparison with observational data. Our experiment improved the mean value slightly rather than completely. Since the ocean seasonal cycle of heat content at mid-latitudes is controlled primarily by surface heat flux (for example, see [33]), the thermal characteristics of the model can apparently be improved through advanced parameterizations for surface flows and vertical mixing. An increased relaxation can also have a positive effect, but this is an artificial method and cannot be used in calculations with a fully interactive model of the atmosphere. Finally, the fact that most models underestimate the maximum summer surface temperature testifies that there can be errors in the external forcing.

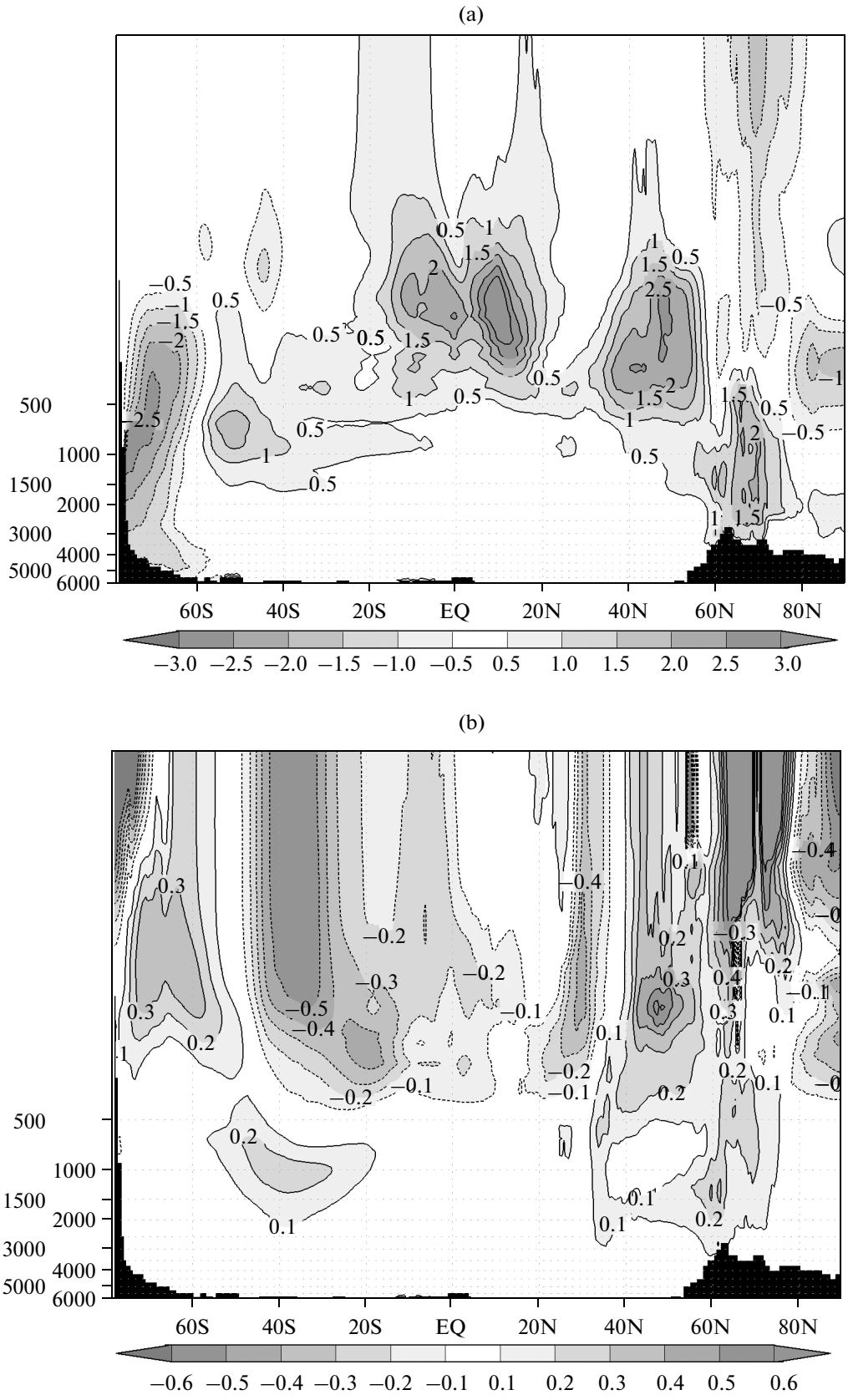

Fig. 4. Zonal averages of deviation of (a) temperature (°C) and (b) salinity (psu) from the WOA2009 annual average climatology (as a function of latitude and depth).

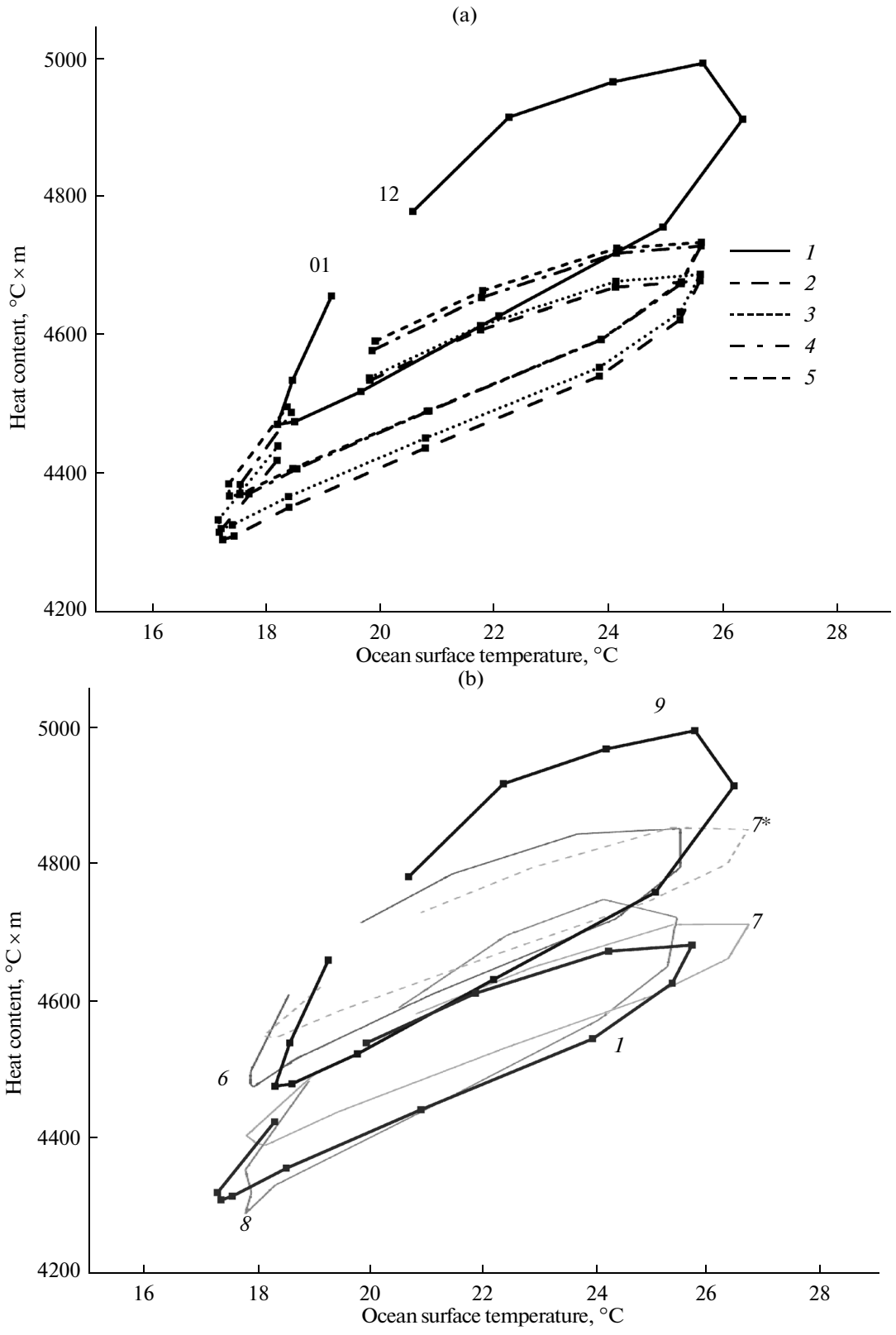

Fig. 5. Dependence of heat content of the upper 250-m layer on ocean surface temperature; monthly averages (01–12). (a) WOA2009 data (*1*) and the number of integration year for the INM–IO model: year 50 (*2*), year 100 (*3*), year 200 (*4*), and year 500 (*5*). (b) WOA2009 data and the 50th year of model of integration. The numbering of models is the same as in Fig. 1; *7** is the MPI model with a strong relaxation and *9* is WOA2009.

4.5. Ice Cover Area

Simulation of high-latitude processes, such as the seasonal cycle of sea ice, is one of the most difficult problems for numerical modeling and an explanation of its results because these processes are very sensitive to external atmospheric influence and to model parameters. This section considers only one of the characteristics of the model climate: the sea ice concentration in the months of its maximum and minimum. Figure 6 shows the field of ice concentration in the Arctic and Antarctic for March (with a maximum in the Northern Hemisphere and a minimum in the South Hemisphere) and September (with a minimum in the Northern Hemisphere and a maximum in the South Hemisphere). The left column shows the fields calculated with the INM–IO model for March 15 and September 15 and the right column shows the data described in [34] for the same months. The total annual mean sea ice area reaches a quasi-equilibrium value over the 10 first years of the experiment for the Northern Hemisphere and over the 50 years for the Southern Hemisphere.

For the Arctic in winter, the model shows a good agreement with observed data except for a slight difference near the southern boundary of ice propagation in near-polar regions of the Atlantic and Pacific oceans. It can be concluded that the ice conditions of the area in this season are most stable with respect to parameters of the experiment and can be qualitatively reproduced even with a simple thermodynamic model of ice. On the contrary, during the Arctic summer, the ice formed in the winter is melted incompletely; therefore, there is too much multiyear ice and our model considerably overestimates ice cover. This season turned out to be also problematic for the group of models described in [21], which were characterized by a largely scattered and generally underestimated ice area (except for the MPI model).

For the final period of the warm season in the Antarctic, the model results are qualitatively consistent with observational data, with the largest deviation in the Ross Sea and an overestimated (on the mean) ice concentration in areas covered by ice. At the same time, the area of the model ice formed during the cold season is smaller than the ice area observed in nature due to both incorrectly ice-free areas and underestimated ice concentration.

4.6. Equatorial Section in the Pacific

The realistic simulation of near-surface characteristics of the tropical Pacific is important for interpreting the El Niño–Southern Oscillation processes. In this section we verify the model on the basis of observational data [35] taken from the review [21].

Figure 7 shows the structure of zonal currents on the equator in the Pacific. According to observational data, the maximum velocity of the Equatorial Countercurrent exceeds 1 m/s, while the model yields a value that is approximately two times lower; here, the countercurrent core turns out to be shifted westward. Most likely these errors are caused primarily by the resolution insufficiency and inaccuracy in the description of vertical mixing, which manifested itself in the eastern (less deep) part of the countercurrent. However, the total flow of the model countercurrent (through the meridian 140° W, in the "corridor" from 3° S to 3° N, and between 60 and 440 m in depth) is 33 Sv, which is very consistent with estimates from observational data (for example, 39 Sv at 140° W [36]). Qualitatively, the model simulates the observed local maxima of the current velocity near 155° E and 145° E. An overestimated velocity of the surface westward current at the east of the section is observed in this experiment like in all experiments of the review [21], which is probably caused by errors in the wind field.

4.7. Mixed Layer Depth

The surface mixed layer of the ocean (SML) is generated by wind, Ekman subduction, and convective instability. The distribution of its maximum depths reached over the year is closely associated with the formation of deep water masses and with the exchange of heat, fresh water, and carbon dioxide. The deep convection zones in the North Atlantic and the Weddell Sea are key elements of the "global ocean conveyor belt."

Different studies use slightly different criteria for determining the SML depth. Since the SML includes small vertical gradients of temperature, salinity, and density, most of the criteria determine the lower boundary of the SML as a level at which the gradients of temperature, density, or buoyancy, or their deviations from the surface values reach given threshold values. We use the criterion described in [37]: the threshold value is taken to be the deviation of potential density by 0.125 σ-units.

The climatological distribution of maximal SML depths is constructed on the basis of monthly fields of temperature and salinity (Fig. 8b). This calculation has the potential to underestimate the actually existing depths because these fields have been smoothed initially and have a data deficit for the cold season due to difficulties in measurements. However, according to [21], climatology generally yields a correct large-scale estimate coinciding with the available data of Argo buoy measurements and WOCE sections, except for the northern margins of the Atlantic and the Labrador Sea, where the climatological mixing depths are underestimated.

It can be seen from Fig. 8 that the INM–IO model qualitatively simulates the boundaries of deepwater formation in the Labrador and Greenland seas as well as near the northwestern coast of the Pacific and in the Mediterranean (overestimated). The deep SML in the Weddell gyre is simulated. For this area, it looks likely

(a)

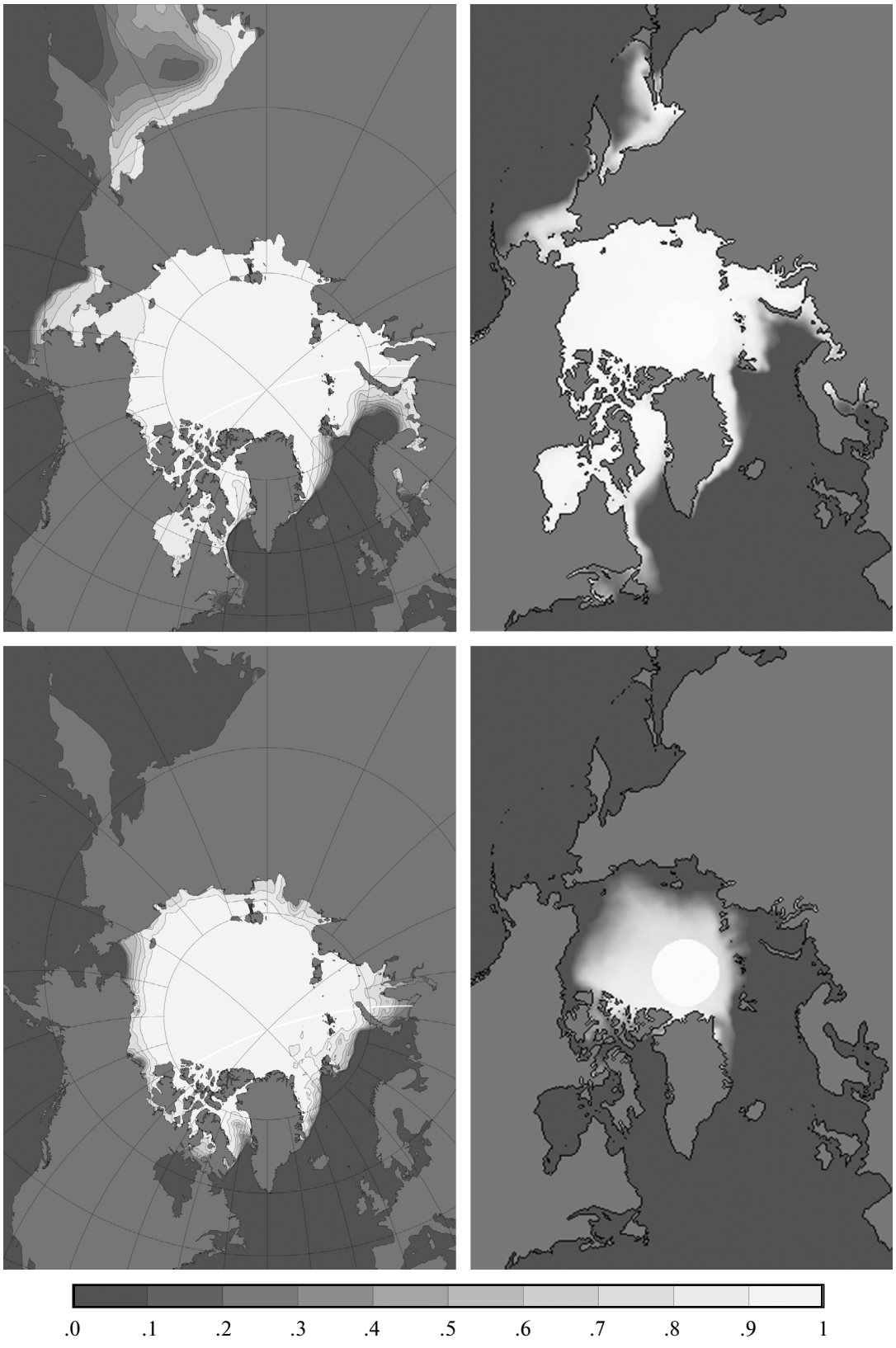

Fig. 6. (a) Sea-ice concentration in the Arctic in March (top) and September (bottom). Results of the INM–IO model (left column) and data of [34] (right column). (b) Same as Fig. 6a except for Antarctica.

(b)

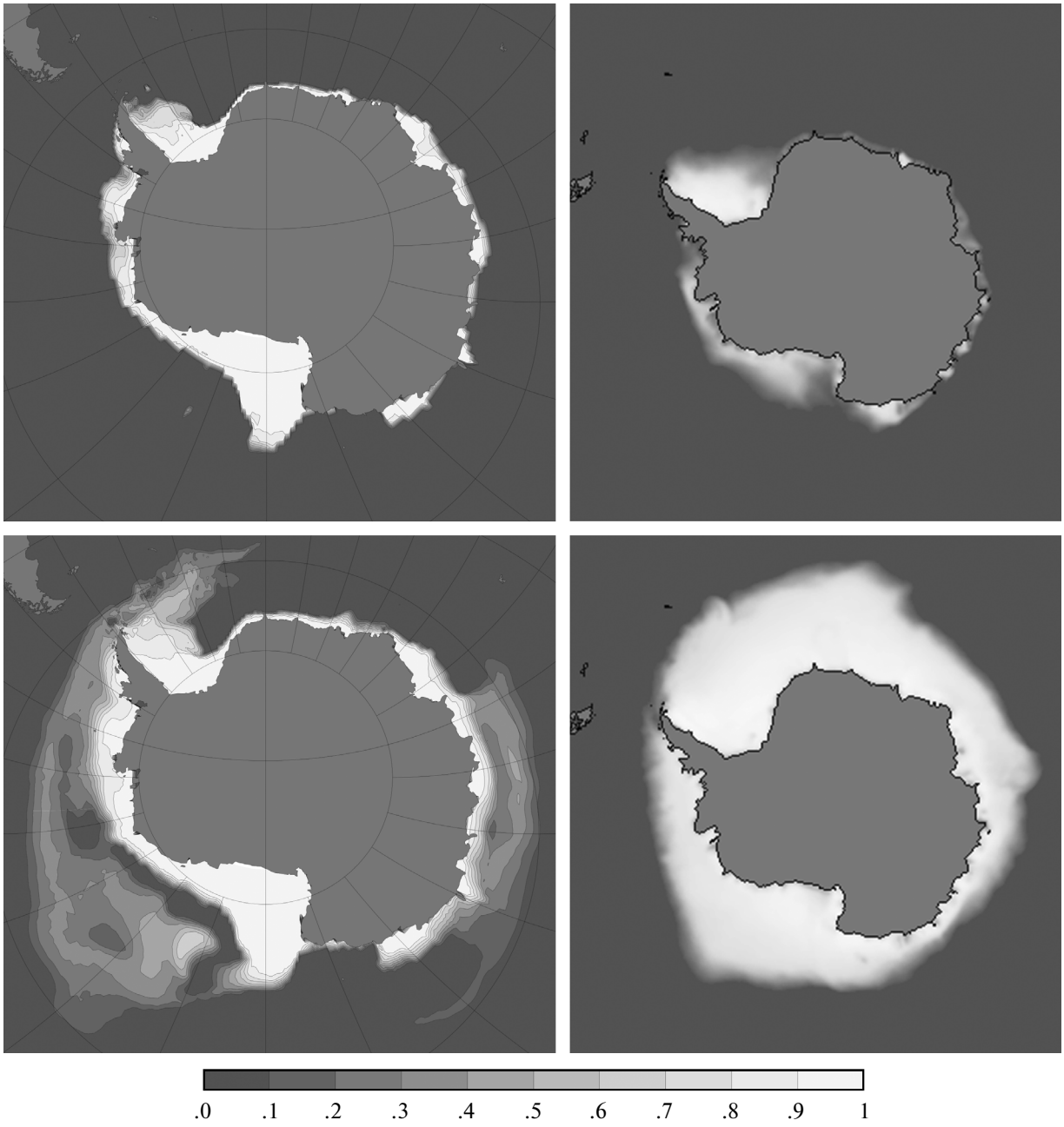

Fig. 6. (Contd.)

that the choice of the criterion for determining the SML depth is important because the method based on the buoyancy deviation for the WOA2005 climatology [21] revealed no deep mixed layer in the central part of the gyre.

The wide and deep SML along the remaining Antarctic coast points to a highly overestimated rate of the meridional overturning circulation and the formation of Antarctic deepwater. The northern boundary of its deepest part (>1500 m) almost coincides with the actually observed position of the southern front of the Antarctic Circumpolar Current [38]. The deep mixed layer (pycnostad) observed on the northern edge of this current and reflecting the formation of the sub-Antarctic water mass is simulated relatively well by our model in the Indian Ocean and western Pacific but is almost absent in the eastern Pacific. As is shown in [21], the numerical models generally fail to simulate this feature.

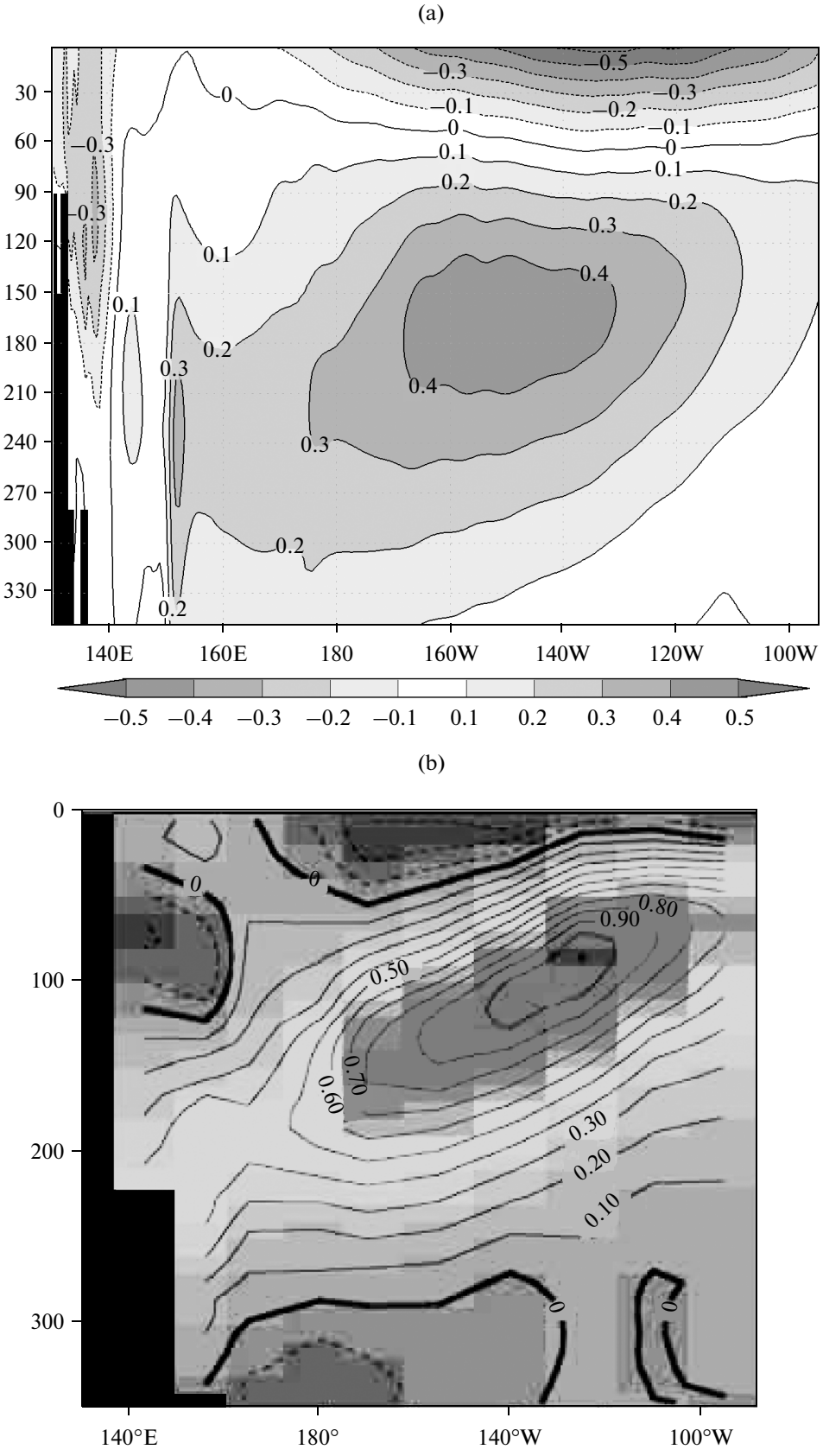

Fig. 7. Zonal component of velocity (m/s) in the upper 350-m layer on the equator in the Pacific. Results of the INM–IO model (a) and data of [35] (b).

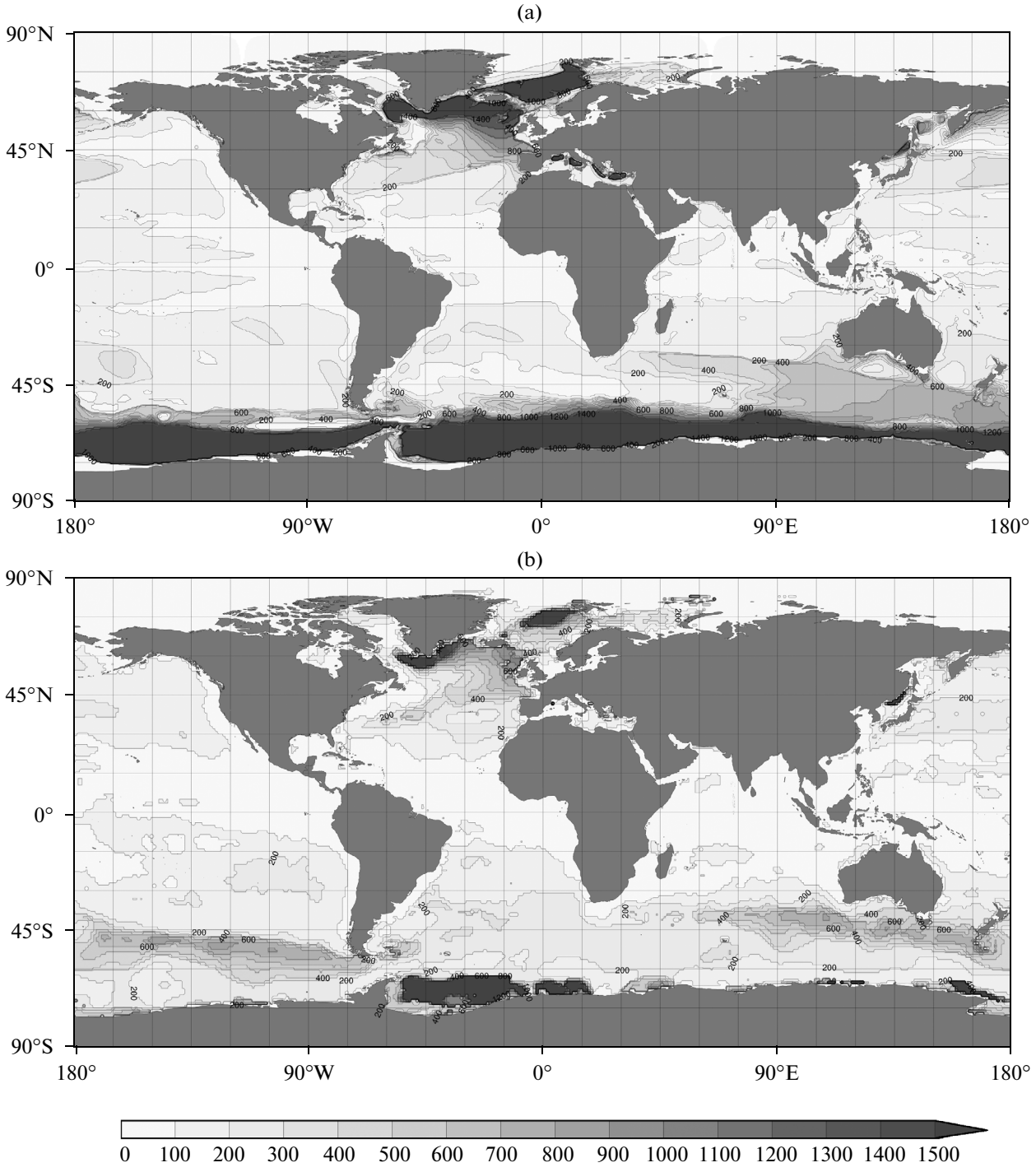

Fig. 8. Distribution of mixed layer depths (m). Maximum of instantaneous values for 491–500 years of the experiment with the INM–IO model (a) and maximum based on WOA2009 monthly mean temperature and salinity fields (b).

4.8. Meridional Heat Transport

Meridional heat transport (MHT) in the Earth's climate system is conditioned by nonuniform heating when tropical areas absorb solar radiation while polar regions emit thermal radiation. A number of studies found that it is highly important to adapt the meridional heat transport by the ocean with flows on the ocean–atmosphere boundary to ensure that model system climate is stable (for example, see [39] and references therein).

Figure 9 shows the plots of global northward MHT obtained with INM–IO and models of the review [21], its separation in our experiment into an explicit

(advection) and subgrid (diffusion) components, and an estimate [40] from observational and reanalysis data. For INM–IO and most models of [21], MHT is calculated explicitly. Only for MPI and MICOM is the heat transport determined from mean heat fluxes on the ocean–atmosphere boundary. Since the horizontal resolution of most models of [21] is around 1°, the INM–IO model data were averaged over 1° cells before the comparison.

The result of our model is generally close to the data of [40]. At most latitudes, the difference does not exceed the uncertainty in these data or the difference between various databases (for example, the climatology of shipboard observations [41] shows that the northward heat transport in tropical and mid-latitudes of the Southern Hemisphere is larger by 0.4 PW). The heating of tropics defined as the MHT difference between 20° N and 20° S was 2.9 PW for the range of estimates from 2.0 PW ([21] on the basis of [23]) to 3.5 PW [40].

An exception was the Southern Ocean, where the model heat transfer reaches significantly overestimated values due to the subgrid component. In addition, the subgrid component is largely responsible for the sharp minimum of MHT at around 40° N. In both cases, errors occur in areas where the MHT is nonmonotonic; therefore, it can be assumed that it is here that the correct description of vortex dynamics by the model is most important. This requires an increased resolution and/or more detailed parameterizations of turbulence.

4.9. Meridional Overturning Circulation

Figure 10 shows the distributions of the stream function of the meridional overturning circulation built from the velocity field of the model solution for the World Ocean and the Atlantic. The value of the function at a point of the plot is the integral southward water transport at the given latitude through the vertical section from the bottom to a given depth.

The distribution and values of the stream function qualitatively coincide with those obtained traditionally with z-coordinate models of the same resolution (for example, [9, 21]). The model simulates wind circulation cells in the upper ocean layer, the powerful deepwater Deacon cell associated with the Antarctic Circumpolar Current and supported by westerly winds, the northern thermohaline cell driven mainly by water downwelling in the North Atlantic, the cell of the Antarctic bottom water mass, and the Abyssal cell near 20° S.

The intensity of tropical wind cells reaches 63 Sv at 3° S and 53 Sv at 3° N. In comparison with the eddy-resolving experiment [9], these cells that were obtained were almost twice as intense and pressed to the equator. However, the intense upwelling in equatorial areas was not simulated, presumably because of the insufficient resolution. The intensity of the northern subpolar wind cell was 6 Sv at latitude 39° N, which almost coincides with the result of the mentioned study.

The Deacon Cell in the Southern Ocean reaches a depth of 3500 m and an intensity of 20 Sv. For [9], the respective values were 3000 m and 34.5 Sv. In [21], most models yielded values of 20–25 Sv; however, it should be taken into account that this quantity involves subgrid circulation parameterized by the Gent–McWilliams method and having an opposite sign to the explicit one.

The circulation of Antarctic bottom water reaches an intensity of 25 Sv at 67° S, which is a significantly overestimated value in comparison with both the coarse z models of [21] (5–10 Sv) and the eddy-resolving calculation [9] (up to 4 Sv). The Abyssal Cell yields 21 Sv at 22° S, which lies on the upper boundary of the scatter by the remaining models and, according to [21], is very consistent with estimates from observational data.

The thermohaline cell associated with the deepwater Atlantic water mass (Fig. 10b) yields a maximum transfer of 24 Sv at a depth of approximately 1000 m, which almost coincides with calculated data [5] (23.9 Sv, 1140 m), slightly exceeds [9] (17.4 Sv, 900 m), and exceeds the estimates from observational data (15 Sv in [21]). According to [21], this intensity turns out to be very sensitive to the model configuration. In addition, the maximum obtained with a coarse resolution is found to be shifted northward (46° N in our model, 33.2° N in [5], and 30° N in [9]).

4.10. Flows of Some Currents

In this section we analyze the mean flows of some currents to estimate the quality of modeling.

The Drake Passage is the narrowest meridional section of the Antarctic Circumpolar Current. The amount of water flowing through this passage is estimated by various methods and observational data to be from 100 Sv [38] to 135 Sv [42]. This value depends in a complicated way on wind influence, baroclinicity, and distribution of pressure gradients; therefore, model verification at this stage is only possible at a qualitative level with respect to this parameter. In our experiment the flow of the Antarctic Circumpolar Current in the Drake Passage was 185 Sv, which significantly exceeds the observed value but falls on the upper limit of the range of model results of [21]. In this case, the model solution obtained in the experiment had a sharp runup to 215 Sv by the 9th year, with a subsequent decline to 177 Sv by the 150th year and reaching to the quasi-steady state level of 185 Sv by the 320th year. A similar result (180–185 Sv) was obtained in [21] by the MPI model using (like INM–IO) a weak relaxation of surface salinity. In a similar experiment with a strong relaxation (50 m/300 days), the MPI model yielded a flow of 135 Sv.

As was noted above, the flow of the Pacific equatorial countercurrent (the Cromwell Current) calculated by the model was around 33 Sv with a measured value

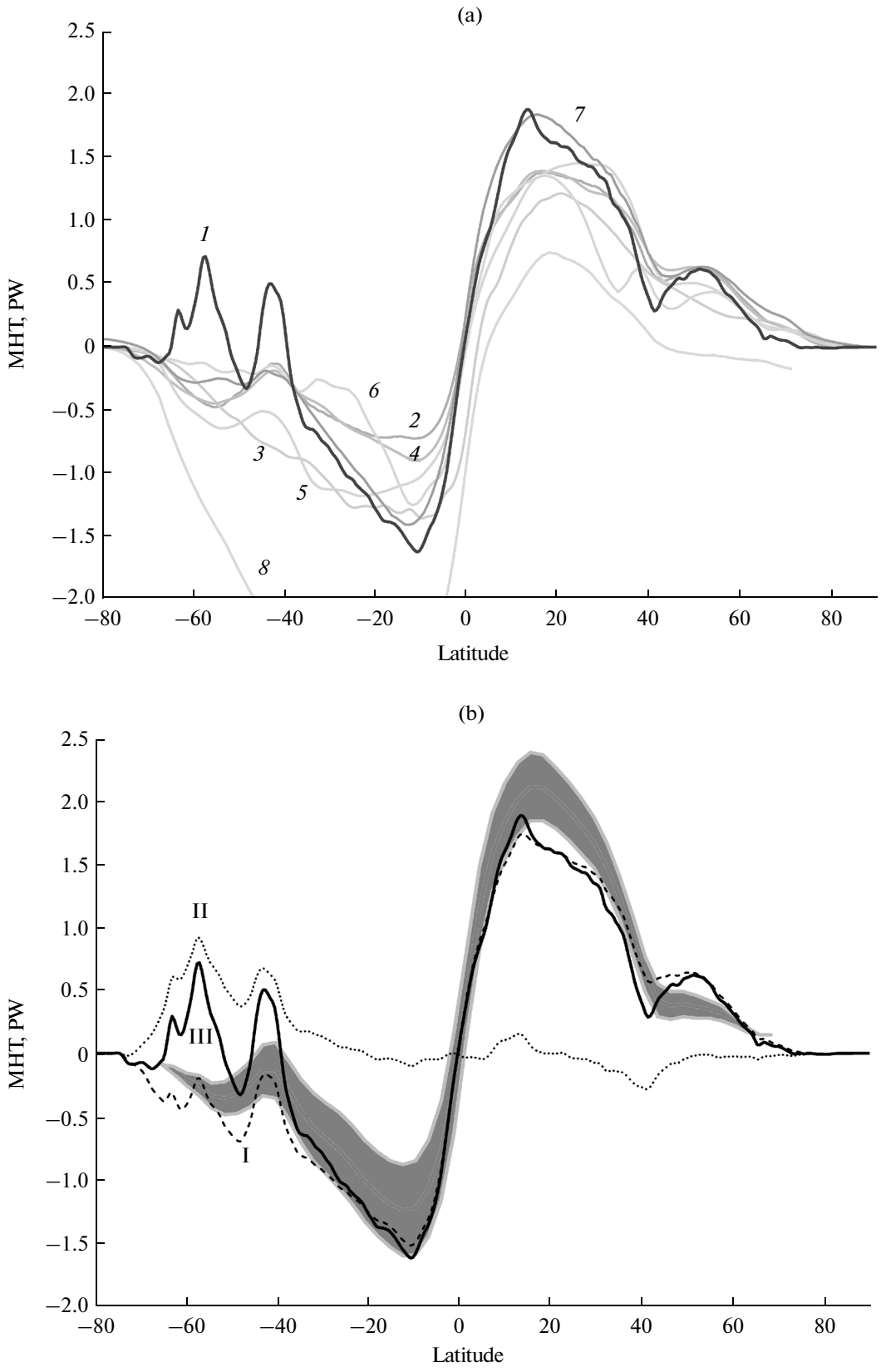

Fig. 9. Meridional heat transport according to INM–IO. (a) Comparison with models of [21]. The numbering of models is the same as in Fig. 1. (b) Ratio of explicit (I) and subgrid (II) components of total (III) heat transport; estimate (corridor) according to data of [40].

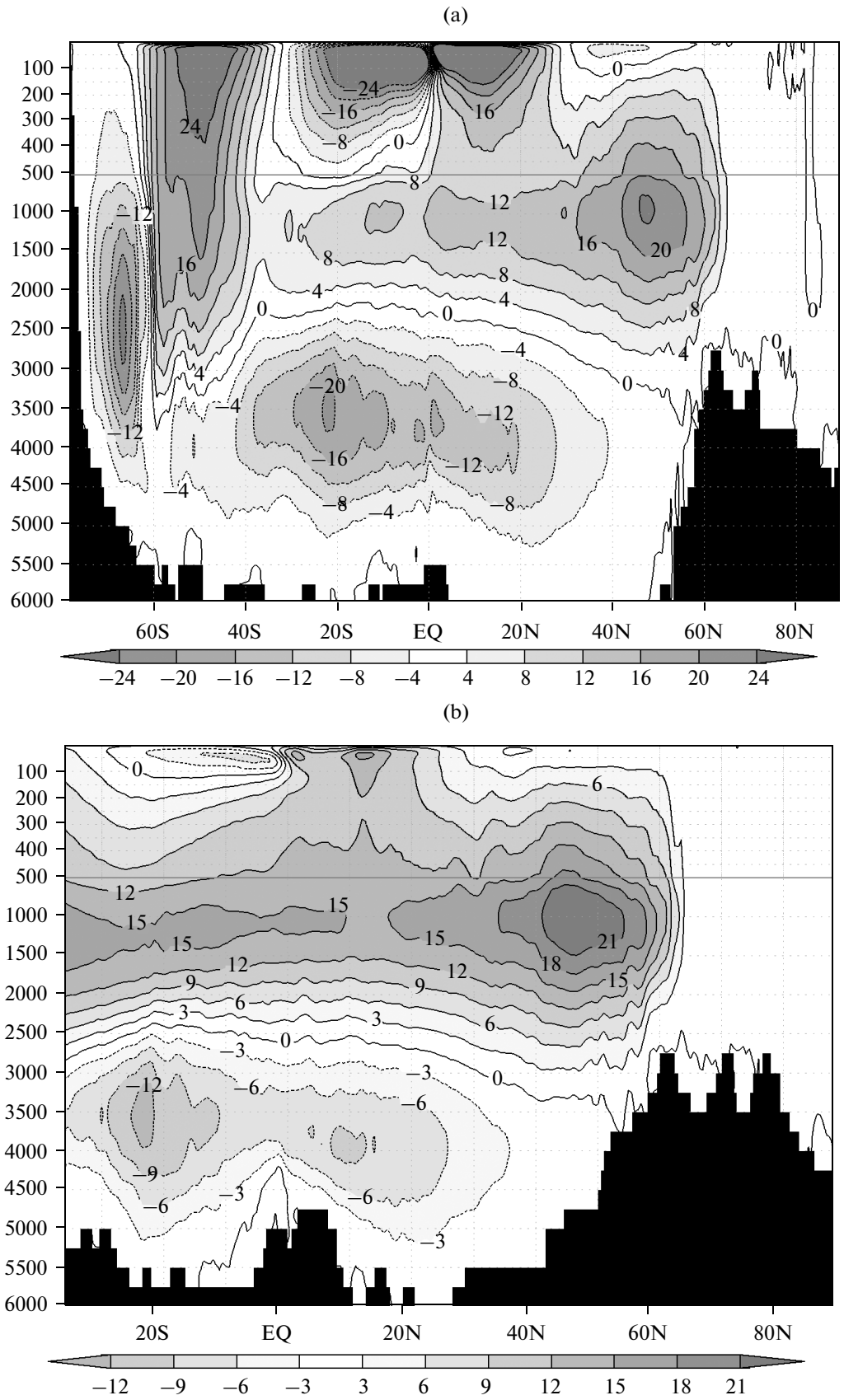

Fig. 10. Stream function of meridional overturning circulation (Sv) obtained by the INM–IO model as a function of depth and latitude for the World Ocean (a) and the Atlantic (b).

of 39 Sv. For the Equatorial countercurrent in the Atlantic Ocean (the Lomonosov Current), the model yields 13 Sv on the meridian 30° W on the lower bound of the estimate from observational data 20.7 ± 6.9 Sv [43].

In the numerical experiment, the rate of the flow to the Arctic through the Bering Strait was 1.4 Sv. According to measurement data [44], the flow averaged over 1991–1994 is 0.83 Sv, with a large interannual variability of up to 50% of the mean value. The eddy-resolving calculation [8] for the same years yielded a value of around 1 Sv with flow fluctuations from –1 to 2 Sv.

The flow from the Arctic through the Fram Strait was 1.7 Sv in our experiment and 1.8 Sv in [8]. In both cases the flow is close to the lower bound of 1997–1999 observation data [45] (4.2 ± 2.3 Sv).

A large number of measurements were conducted for the Gulf Stream in its different areas. We limit ourselves to the flow near the Cape Hatteras. This numerical experiment yielded a flow of 39 Sv, while the measured value was 65 Sv [46]. A more detailed study of the Gulf Stream structure is planned in subsequent calculations using the INM–IO model with an eddy-resolving resolution.

5. CONCLUSIONS

The quasi-equilibrium state of the ocean obtained in the numerical experiment is the own climate of the INM–IO model. Despite the fact that this state was calculated with a sufficiently coarse resolution and using simple parameterizations, the experiment showed that the model is appropriate for simulating large-scale oceanic processes. The experiment provided an original view of the mechanisms controlling the model climate and made it possible to identify the lines for further improvement of the model. The practical results of the experiment can be formulated as the following conclusions.

(1) When a conservative and not overly viscous advection scheme is used, the mean temperature of the ocean quickly becomes stabilized. To conserve mean salinity, it is very important to balance the ice model in a way that prevents its drift. The character of the vertical distribution of temperature and salinity is largely determined by the type of vertical coordinates used in the model.

(2) When a coarse spatial resolution is used in the model, the largest errors in the distribution of temperature and salinity occur in the areas of coastal jet current and upwelling. The accuracy of the simulation of the thermohaline structure of Arctic regions significantly depends on the ice model accuracy and the setup of the salinity relaxation scheme. The Southern Ocean turned out to be the most difficult among planetary basins for both modeling and obtaining estimates from observational data; presumably, this happens primarily due to complexity in the vortex dynamics of the Antarctic Circumpolar Current.

(3) Model solutions proved to be highly smoothed even in comparison with climatology, which can be caused by both the low resolution of atmospheric forcing and the model ocean viscosity. The flows of the currents are qualitatively simulated, while the flows for jet currents are underestimated. The intensity of large-scale elements of the circulation can be overestimated or underestimated.

(4) In terms of many parameters, the results were close to those obtained with the MPI model, which uses a vertical grid and salinity relaxation scheme similar to our model.

(5) The reasons for a given error in the model solution cannot be always clearly established. The errors of even low-resolution models are often comparable with the uncertainty of observational data.

Further activities with the model will be related to calibration, the improvement of parameterizations and submodels (specifically, the submodels of ice and vertical mixing), transition to a high resolution, and numerical implementation on a C-grid.

ACKNOWLEDGMENTS

This study was supported by the Russian Science Foundation, project no. 14-27-00126, and conducted in the Institute of Numerical Mathematics, Russian Academy of Sciences.

REFERENCES

1. A. S. Sarkisyan, *Theory and Computation of Ocean Currents* (Gidrometeoizdat, Leningrad, 1966; Israel Program for Scientific Translations, Jerusalem, 1969).
2. G. I. Marchuk, *Numerical Solution of Problems of Atmospheric and Oceanic Dynamics* (Gidrometeoizdat, Leningrad, 1974) [in Russian].
3. A. S. Sarkisyan, "“Fifty years of numerical modeling of baroclinic ocean,” Izv., Atmos. Ocean. Phys. **48** (1), 1–14 (2012).
4. *Climate Change 2013: The Physical Science Basis—Contribution of Working Group I to the Fifth Assessment Report of the Intergovernmental Panel on Climate Change*, Ed. by T. F. Stocker, D. Qin, G.-K. Plattner, et al. (Cambridge University Press, Cambridge, 2013).
5. R. D. Smith, M. E. Maltrud, F. O. Bryan, and M. W. Hecht, “Numerical simulation of the North Atlantic Ocean at 1/10°,” J. Phys. Oceanogr. **30**, 1532–1561 (2000).
6. E. P. Chassignet and D. P. Marshall, “Gulf Stream separation in numerical ocean models,” in *Ocean Modeling in an Eddying Regime*, Ed. by M. W. Hecht and H. Hasumi (American Geophysical Union, Washington, DC, 2008), pp. 39–61.
7. Y. S. Chang, Z. D. Garraffo, H. Peters, and T. M. Özgökmen, “Pathways of Nordic Overflows from climate model scale and eddy resolving simulations,” Ocean modeling **29**, 66–84 (2009).
8. M. E. Maltrud and J. L. McClean, “An eddy resolving global 1/10° ocean simulation,” Ocean Modell. **8**, 31–54 (2005).
9. Y. Masumoto, H. Sasaki, T. Kagimoto, et al., “A fifty-year eddy-resolving simulation of the world ocean—

Preliminary outcomes of OFES (OGCM for the Earth Simulator)," J. Earth Simul. **1**, 35–56 (2004).
10. A. M. Treguier and B. Barnier, DRAKKAR, Coordination of high resolution global ocean simulations and developments of the NEMO modelling framework, Project INSU–LEFE and GMMC report of activity 2010–2012 (2010).
11. A. V. Gusev and N. A. Diansky, "Numerical simulation of the World Ocean circulation and its climatic variability for 1948–2007 using the INMOM," Izv., Atmos. Ocean. Phys. **50** (1), 1–12 (2014).
12. R. A. Ibrayev, "Model of enclosed and semi-enclosed sea hydrodynamics," Russ. J. Numer. Anal. Math. Modell. **16** (4), 291–304 (2001).
13. P. D. Killworth, D. Stainforth, D. J. Webb, and S. Paterson, "The development of a free surface Bryan–Cox–Semtner model," J. Phys. Oceanogr. **21**, 1333–1348 (1991).
14. V. V. Kalmykov and R. Ibrayev, "The overlapping algorithm for solving shallow water equations on massively-parallel architectures with distributed memory," Vestn. Ufim. Gos. Aviats. Tekh. Univ. **17** (5), 252–259 (2013).
15. V. V. Kalmykov and R. A. Ibrayev, "A framework for the ocean-ice-atmosphere-land coupled modeling on massively-parallel architectures," Vychisl. Metody Program. **14**, 88–95 (2013).
16. V. V. Kalmykov and R. A. Ibrayev, "Software for combined modeling of the ocean–ice–atmosphere–soil system on massively parallel computers," Certificate of state registration of computer programs No. 2013619320, Russia (October 1, 2013).
17. V. V. Kalmykov, Extended Abstract of Candidate's Dissertation in Mathematics and Physics (Institute of Numerical Mathematics, Russian Academy of Sciences, Moscow, 2013).
18. M. A. Tolstykh, R. A. Ibrayev, E. M. Volodin, et al., *Models of the Global Atmosphere and World Ocean: Algorithms and Supercomputer Technologies* (MGU, Moscow, 2013) [in Russian].
19. R. A. Ibrayev, V. V. Kalmykov, K. V. Ushakov, and R. N. Khabeev, "Eddy-resolving 1/10° model of the World Ocean," Ekol. Bezop. Pribrezhn. Shel'f. Zon Kompleksn. Ispol'z. Resur. Shel'fa **25** (2), 30–44 (2011).
20. R. A. Ibrayev, R. N. Khabeev, and K. V. Ushakov, "Eddy-resolving 1/10° model of the World Ocean," Izv., Atmos. Ocean. Phys. **48** (1), 37–46 (2012).
21. S. M. Griffies, A. Biastoch, C. Boning, et al., "Coordinated ocean–ice reference experiments (COREs)," Ocean Modell. **26** (1–2), 1–46 (2009).
22. C. Schrum and J. Backhaus, "Sensitivity of atmosphere–ocean heat exchange and heat content in North Sea and Baltic Sea. A comparative assessment," Tellus, **51A**, 526–549 (1999).
23. W. Large and S. Yeager, Diurnal to decadal global forcing for ocean and sea-ice models: the data sets and flux climatologies, NCAR Technical Note: NCAR/TN-460+STR (CGD Division of the National Center for Atmospheric Research, 2004).
24. W. H. Munk and E. R. Anderson, "Note on the theory of the thermocline," J. Mar. Res. **7**, 276–295 (1948).
25. S. T. Zalezak, "Fully multidimensional flux-corrected transport algorithm for fluids," J. Comput. Phys. **31**, 335–362 (1979).
26. W. Large and S. Yeager, "The global climatology of an interannually varying air–sea flux data set," Clim. Dyn. **33** (2–3), 341–364 (2009).
27. M. Steele, R. Morfley, and W. Ermold, "PHC: A global ocean hydrography with a high-quality Arctic Ocean," J. Clim. **14**, 2079–2087 (2001).
28. World Ocean Atlas 2009. http://www.nodc.noaa.gov/OC5/WOA09/pr_woa09.html.
29. R. J. Murray, "Explicit generation of orthogonal grids for ocean models," J. Comput. Phys. **126** (2), 251–273 (1996).
30. ETOPO5. Data Announcement 88-MGG-02. Digital relief of the surface of the Earth. (National Geophysical Data Center, NOAA, Colorado, 1988).
31. M. Conkright, J. Antonov, O. Baranova, et al., *World Ocean Database 2001*, Vol. 1: *Introduction. NOAA Atlas NESDIS 42* (NOAA, Washington, DC, 2002).
32. R. W. Reynolds and T. M. Smith, "Improved global sea surface temperature analyses using optimum interpolation," J. Clim. **7** (6), 929–948 (1994).
33. J. L. Sarmiento, "On the North and Tropical Atlantic heat balance," J. Geophys. Res. **91** (C10), 11677–11690 (1986).
34. J. Stroeve, *Sea Ice Trends and Climatologies from SMMR and SSM/I-SSMIS (Updated Dataset for 1979–2013)* (NASA DAAC at the National Snow and Ice Data Center, Boulder, Colorado, 2003).
35. G. C. Johnson, B. M. Sloyan, W. S. Kessler, and K. E. McTaggart, "Direct measurements of upper ocean currents and water properties across the tropical Pacific during the 1990s," Prog. Oceanogr. **52**, 31–36 (2002).
36. J. A. Knauss, "Measurements of the Cromwell Current," Deep-Sea Res. (1953) **6**, 265–274, IN25–IN26, 275–286 (1959–1960).
37. G. Monterey and S. Levitus, *Climatological Cycle of Mixed Layer Depth in the World Ocean* (NOAA NESDIS, Washington, DC, 1997).
38. A. H. Orsi, T. W. Whitworth III, and W. D. Nowlin, Jr., "On the meridional extent and fronts of the Antarctic Circumpolar Current," Deep-Sea Res. **42** (5), 641–673 (1995).
39. C. Gordon, C. Cooper, C. A. Senior, et al., "The simulation of SST, sea ice extents and ocean heat transports in a version of the Hadley Centre coupled model without flux adjustments," Clim. Dyn. **16**, 147–168 (2000).
40. K. Trenberth and J. Caron, "Estimates of meridional atmosphere and ocean heat transports," J. Clim. **14**, 3433–3443 (2001).
41. A. M. Da Silva, C. Young, and S. Levitus, Atlas of surface marine data. NOAA Atlas NESDIS 6 (1994).
42. S. Cunningham, S. Alderson, B. King, and M. Brandon, "Transport and variability of the Antarctic Circumpolar Current in Drake Passage," J. Geophys. Res. **108** (C5), 8084 (2003).
43. E. J. Katz, R. L. Molinari, D. E. Cartwright, et al., "The seasonal transport of the Equatorial Undercurrent in the western Atlantic (during the Global Weather Experiment)," Oceanol. Acta **4** (4), 445–450 (1981).
44. A. T. Roach, K. Aagaard, C. H. Pease, et al., "Direct measurements of transport and water properties through the Bering Strait," J. Geophys. Res.: Oceans **100** (18), 443–458 (1995).
45. E. Fahrbach, J. Meincke, S. Osterhus, et al., "Direct measurements of volume transports through Fram Strait," Polar Res. **20**, 217–224 (2001).
46. J. A. Knauss, "A note on the transport of the Gulf Stream," Deep-Sea Res. **16 (Suppl.)**, 117–123 (1969).

Translated by V. Arutyunyan